

## The 2007 Kahak and 2010 Kazerun Earthquakes: Constrained Non-Negative Least-Squares Linear Finite Fault Inversion for Slip Distribution

Bazargan, S.<sup>1</sup>, Shomali, Z. H.<sup>2\*</sup> and Rezapour, M.<sup>3</sup>

1. M.Sc. Graduated, Department of Seismology, Institute of Geophysics, University of Tehran, Tehran, Iran

2. Associate Professor, Department of Seismology, Institute of Geophysics, University of Tehran, Tehran, Iran

3. Professor, Department of Seismology, Institute of Geophysics, University of Tehran, Tehran, Iran

(Received: 29 May 2020, Accepted: 24 Jan 2021)

### Abstract

Here we study slip distribution of the June 18, 2007  $M_w$  5.5 Kahak and September 27, 2010  $M_w$  5.9 Kazerun earthquakes by using constrained non-negative least-squares linear slip inversion method for regional broadband seismic data. Hundreds of inversions were carried out to obtain the optimal parameters used in the process, including rupture velocity and rise time. We used the rupture velocity of 2.6 km/s (0.75  $V_s$ ) and the rise time of 1.4 s for the first event, and 2.8 km/s (0.75  $V_s$ ) and 2.1 s for the second one. Results show the rupture with the peak slip of 8.6 cm and 14.3 cm, and the total seismic moment release of  $1.59 \times 10^{24}$  dyne-cm and  $2.80 \times 10^{25}$  dyne-cm for the Kahak and Kazerun earthquakes, respectively. Owing to the non-uniqueness of the inversion problem, we presented a set of solutions for both events. Furthermore, the sensitivity of the slip models to some influential parameters such as rupture velocity and rise time was explored. Moreover, we used two ways for identifying the main/preferred fault plane, which are compatible with one another: First, discerning the main fault plane by using the slip inversion method; second, distinguishing the main fault plane by the use of aftershocks. To the best of our knowledge, this is the first time to apply the linear finite-fault inversion method to moderate earthquakes in Central Iran and Zagros seismotectonic provinces to model a set of rupture histories at regional distances.

**Keywords:** Kahak earthquake, Kazerun earthquake, seismic data, slip inversion, finite-fault modeling.

### 1. Introduction

The tectonic of Iran is governed by convergent plate collisions along the Alpine-Himalayan active belt (Berberian, 1981; Mirzaei et al. 1998). According to Mirzaei et al. (1998), there are five major seismotectonic provinces in the country, namely Zagros in the southwest, Alborz-Azerbaijan in the north and northwest, Central East Iran, Kopeh Dagh in the northeast, and Makran in the southeast. Subduction of the African-Arabian plate and central Iran creates the 'Zagros suture zone' along the Main Zagros Reverse fault (Berberian, 1981; Mirzaei et al. 1998) where the suture zone separates two different continental blocks (Berberian, 1981), i.e. Central Iran and Zagros seismotectonic provinces. For this study, two earthquakes from these two main seismotectonic provinces are chosen. The first event is the June 18, 2007  $M_w$  5.5 Kahak earthquake, which is sited in Central Iran seismotectonic province in the vicinity of Kahak district of Qom province near Tehran, the capital of Iran (Figure 1). This event caused shaking in Tehran city that is located about 140 km

north of the earthquake epicenter. The second one is the September 27, 2010  $M_w$  5.9 Kazerun earthquake situated in Zagros seismotectonic province, near Kazerun County in Fars Province. This earthquake occurred near the Kazerun fault crossing the Zagros folds (Berberian and Tchalenko, 1976; Berberian, 1995) near the Hormoz Salt Dome.

We study the rupture histories here using the slip inversion method. It has been known for decades that finding seismic slip on an assumed fault plane is an effective way to study the physics of earthquake faulting. More specifically, finite-fault source models provide essential information about earthquake rupture phenomena. For example, they can reveal the space and time evolution of rupture and explain the kinematics of large tectonic earthquake sources. However, finite-fault-rupture models are subject to remarkable uncertainty because of imprecise observations and imperfect Green's functions. Moreover, imaging methods such as back-projection is a common procedure to image detailed processes of faulting. The main

\*Corresponding author:

shomali@ut.ac.ir

challenge of these methods is also their built-in, sometimes subtle, artifacts. Generally, imaging methods can be applied to relatively narrow spectral bands, which gives an uncompleted representation of the rupturing process. Although both back-projection and finite-fault modeling methods have uncertainties in their results, the former provides quick imaging of the rupturing by simplifying or neglecting the source and/or structure complexities. That is why the back-projection methods need a few requirements of prior information of the source complexity. In contrast, more parameters need to be prepared in finite-fault modeling to image the fault slip. Nevertheless, this method helps identify the main fault plane which is of great significance, for the knowledge of causative faults is a key in seismotectonic studies.

The main aim of the present study is to determine, to the degree that the available

data allow, the spatial and spatiotemporal distribution of slip for the 2007 Kahak earthquake and the spatial slip distribution of the 2010 Kazerun earthquake using a linear finite-fault inversion method for seismic data. The seismological data are preferred for investigating slip distribution because of their sensitivity to both the spatial and temporal characteristics of the rupture (Delouis et al., 2002). Since slip inversion problems have no unique solution, many slip models may fit the data in the same way. Furthermore, running inversions with different values of parameters such as rupture velocity and rise time demonstrate significant uncertainties in the slip models. Thus, a set of models can describe the faulting process for a given source. This study sets out to find a group of different models and explore the sensitivity of the preferred models. We also examine the effect of subdividing data set upon the slip distribution.

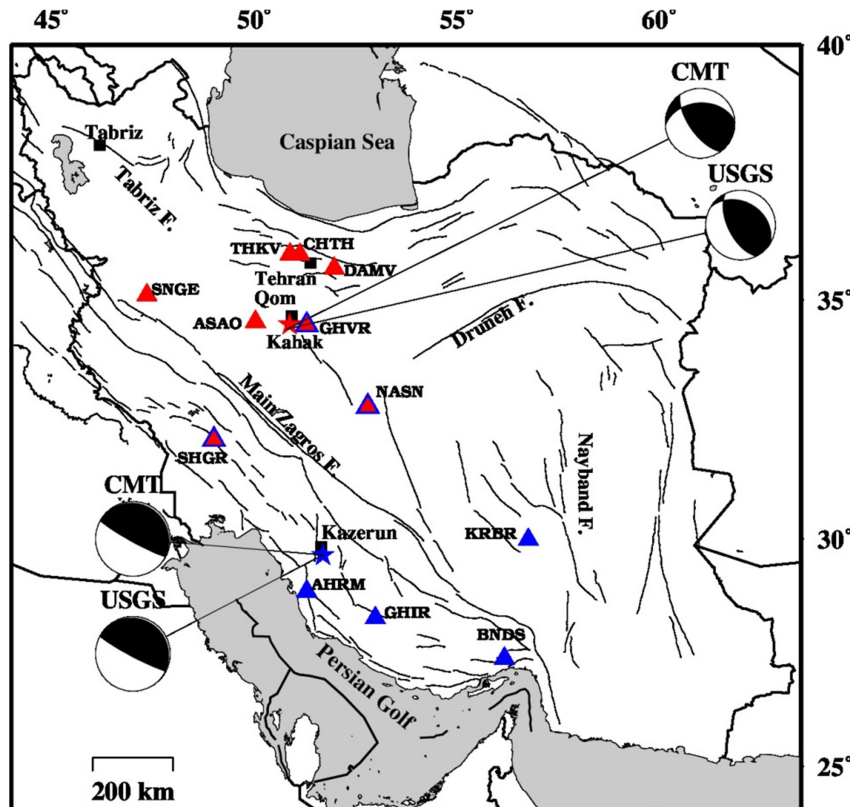


**Figure 1.** Distribution of stations for the Kahak (red triangles) and Kazerun (blue triangles) earthquakes. The Kazerun earthquake has stations GHVR, NASN, and SHGR in common with the Kahak earthquake (the red triangles with blue outlines). The locations of the epicenters are given by the red and blue stars for the Kahak and Kazerun events, respectively. The earthquake focal mechanisms reported by GCMT and USGS are shown for both earthquakes. Solid lines also demonstrate fault traces of Iran. Three major faults of Iran such as Daruneh, Nayband, and Main Zagros faults are illustrated in the figure. Additionally, black squares symbolize towns. The first event is situated in Central Iran seismotectonic province, in the vicinity of Kahak district of Qom province near Tehran, and the second earthquake is sited in Zagros seismotectonic province, near Kazerun County.

## 2. Data

We obtained the seismic data from a national broadband seismic network operated by the International Institute of Earthquake Engineering and Seismology of Iran (IIEES, [www.iiees.ac.ir](http://www.iiees.ac.ir)). These data consist of 24 waveforms for the June 18, 2007  $M_w$  5.5 Kahak earthquake and 20 waveforms for the September 27, 2010  $M_w$  5.9 Kazerun earthquake. Figure 1 displays the location of stations for both earthquakes, and the stations and their epicentral distances are listed in Table 1. The aftershocks of the corresponding earthquakes were also taken from the catalog of the Iranian Seismological Center (IRSC, [irsc.ut.ac.ir](http://irsc.ut.ac.ir)).

In the process of preparing data, we filtered and decimated the observed waveforms from the original 50 to 10 samples per second. Next, we removed the instrument responses, and then we converted the data to displacement. The band-pass filter of 0.03-0.15 Hz for the first event and 0.009-0.08 Hz for the second one were applied to the displacement waveforms.

## 3. Model Parameterization

In this study, we calculated Green's functions using the frequency-wavenumber integration code (FKRPROG) developed by Saikia (1994). Furthermore, the inversion algorithm used for acquiring synthetic data is based on

a stabilized constrained non-negative least-squares method introduced by Hartzell and Heaton (1983).

We obtained optimal values of several parameters as a result of running many inversions. The first parameters creating our parameterization are fault and subfault sizes. In the spatial distribution of the two events, the model parameters compose a single fault segment with smoothing stabilization. On the one hand, large subfaults may cause artifact slip patches, and slip models with the lack of spatial resolution of the fault details can be obtained by a few large subfaults (Hartzell and Heaton, 1983). On the other hand, using very small subfaults may cause completely inaccurate results, and in so doing, artifacts. In this regard, we tested different subfault sizes ranging from 0.5 km to 5.0 km to find the best size. For two reasons, the equal-sized 1 km  $\times$  1 km subfaults with a surface of 34 km by 34 km for the first event and 3 km  $\times$  3 km subfaults with a surface of 60 km by 60 km for the second one were found to be the best choices. The first reason is that these fault and subfault sizes accommodated all of the slip distribution inside the given fault plane. Second, they provided enough resolution of fault details with a maximum percentage of the fit between the observed and synthetic data.

**Table 1.** The stations used in the inversion with their epicentral distances.

Kahak	Earthquake	Kazerun	Earthquake
station	epicentral distance (km)	station	epicentral distance (km)
GHVR	39.37	AHRM	95.76
ASAO	77.47	GHIR	197.08
THKV	157.50	NASN	364.49
CHTH	158.42	SHGR	388.06
DAMV	161.16	KRBR	491.03
NASN	260.47	BNDS	504.32
SHGR	327.28	GHVR	536.50
SNGE	328.82		

Additionally, we prepared a set of solutions because of the non-uniqueness of the inversion problem. That is why we used several hypocentral parameters and focal mechanisms. We tested different hypocenters reported by several seismological agencies, namely ISC, GCMT, USGS, and EMSC (Table 2). Moreover, one nodal plane generating a better fit to the data can be considered as the fault plane (e.g. Abercrombie et al., 2001). Thus, we examined the focal mechanism (strike, dip, and rake) estimated by USGS and GCMT (Table 3) to see which one better fits the waveforms. For both earthquakes, we acquired the slip models for both GCMT and USGS, and the GCMT focal mechanisms, having the best data fit, were construed as the main faults. To put it another way, slip models can aid us to distinguish the fault plane from the auxiliary plane. More specifically, for all hypocentral parameters

(Table 2) of the Kahak earthquake, the inversion found better data fits using the 266° nodal plane of the GCMT solution (Table 3), which was thus considered to be the main fault. Furthermore, the corresponding aftershocks showed in a cross-sectional view (Figure 2a) defined a plane that is compatible with the 266° plane. For the Kazerun earthquake, the GCMT solution with the strike, dip, rake: 301°, 6°, 100° provided the maximum fit between the observed and synthetic waveforms. Thus, this nodal plane was construed as the main fault. In addition, the aftershock distribution approximately aligned along the strike of this nodal plane (Figure 2b), which increased the probability of this nodal plane being the main fault. Consequently, we used these nodal planes for the rest of the investigation. (The measure to choose the optimal results in this study is total variance reduction that demonstrates the fit between the observed and synthetic data).

**Table 2.** The hypocentral parameters recorded by different agencies for the Kahak and Kazerun earthquakes.

2007 Kahak					2010 Kazerun			
Agencies*	Lat. (°)	Lon. (°)	Depth (km)	Time	Lat. (°)	Lon. (°)	Depth (km)	Time
ISC	34.49	50.86	11.0	14 <sup>h</sup> 29 <sup>m</sup> 49 <sup>s</sup> .77	29.65	51.69	21.3	11 <sup>h</sup> 22 <sup>m</sup> 45 <sup>s</sup> .23
GCMT	34.47	50.79	18.5	14 <sup>h</sup> 29 <sup>m</sup> 54 <sup>s</sup> .50	29.56	51.62	17.1	11 <sup>h</sup> 22 <sup>m</sup> 48 <sup>s</sup> .60
USGS	34.43	50.83	5.0	14 <sup>h</sup> 29 <sup>m</sup> 48 <sup>s</sup> .29	29.63	51.66	20.0	11 <sup>h</sup> 22 <sup>m</sup> 45 <sup>s</sup> .18
EMSC	34.51	50.83	25.0	14 <sup>h</sup> 29 <sup>m</sup> 49 <sup>s</sup> .90	29.64	51.63	10.0	11 <sup>h</sup> 22 <sup>m</sup> 43 <sup>s</sup> .70

\* Isc ([www.isc.ac.uk](http://www.isc.ac.uk)), International Seismological Center; GCMT ([www.globalcmt.org](http://www.globalcmt.org)), Global Centroid Moment Tensor; USGS ([www.earthquake.usgs.gov](http://www.earthquake.usgs.gov)), United States Geological Survey; EMSC ([www.emsc-csem.org](http://www.emsc-csem.org)), European-Mediterranean Seismological Centre.

**Table 3.** The focal mechanisms reported by GCMT and USGS.

2007 Kahak	Nodal Plane 1			Nodal Plane 2		
	Strike(°)	Dip(°)	Rake(°)	Strike(°)	Dip(°)	Rake(°)
GCMT	266	41	39	144	66	124
USGS	301	34	62	154	60	108
2010 Kazerun	Nodal Plane 1			Nodal Plane 2		
	Strike(°)	Dip(°)	Rake(°)	Strike(°)	Dip(°)	Rake(°)
GCMT	309	6	100	119	85	89
USGS	316	6	108	118	84	88

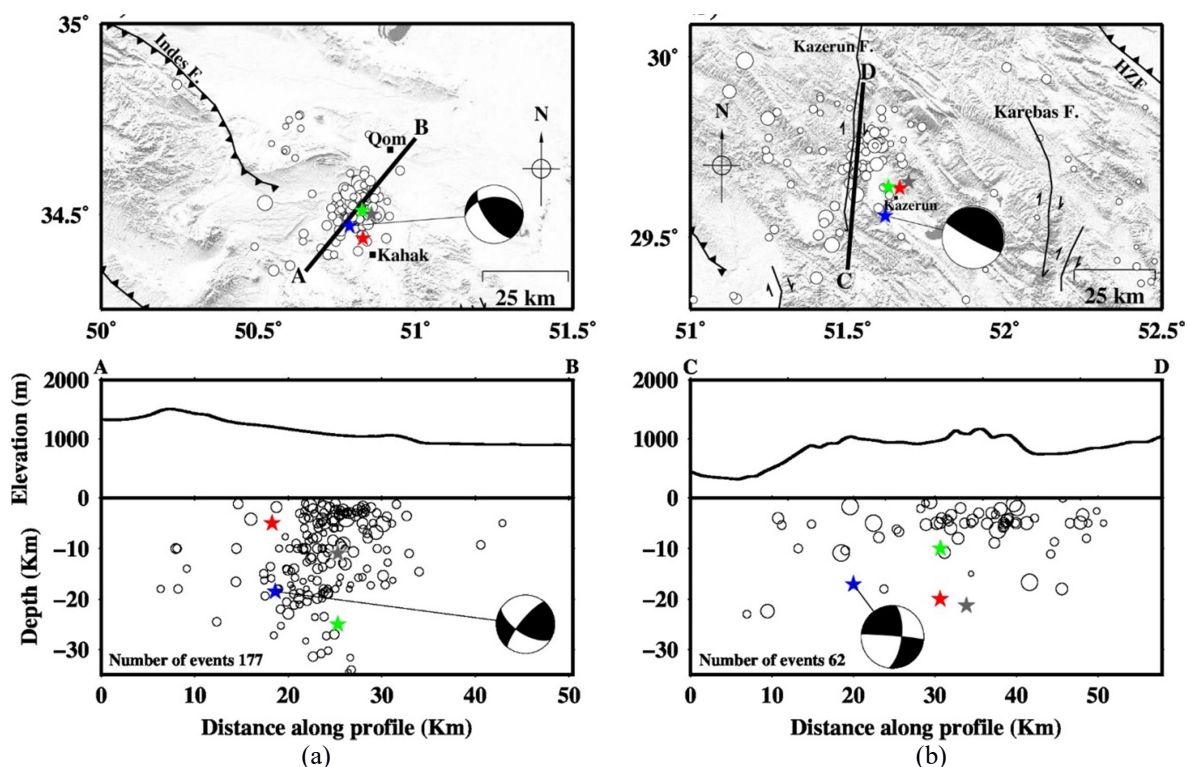


**Figure 2.** The aftershock distribution of the a) Kahak and b) Kazerun earthquakes. Aftershocks were taken from the catalog of the Iranian Seismological Center (IRSC). The white circles refer to the aftershocks occurred during the three months after the mainshock. Red, blue, green, and grey stars denote the hypocenters reported by USGS, GCMT, EMSC, and ISC, respectively, in the map view (top) and the cross-sectional view (bottom). We projected the aftershocks onto a two-dimensional profile—A-B section for the first event (panel a) and C-D section for the second earthquake (panel b). The top panels illustrate the aftershocks and the sections on the surface, and the bottom panels demonstrate them in the cross-section. The focal mechanism of events reported by GCMT in the map view (top) is shown in the cross-sectional view in the bottom panels. Based on the aftershocks trends, the  $266^\circ$  nodal plane (the Kahak earthquake) and the  $301^\circ$  nodal plane (the Kazerun earthquake) were construed as the main fault planes.

The next crucial parameters are the rupture velocity and rise time. The rupture velocity assumed here to be a constant fraction of the shear wave velocity at the source area ranged from 0.7 to 0.9  $V_s$ . Finally, stabilization constraints, namely moment minimization and smooth weight, were considered in the inversion to lower the instability of the models. For this purpose, we tested different amounts of these constraints to find the best values yielding a smooth slip model with the minimum seismic moment (Hartzell and Heaton, 1983).

#### 4. The results of the 2007 Kahak Earthquake

The 2007 Kahak earthquake is of great significance, because, as of 2007, there have not been any similar earthquake bigger than that ( $M_w$  5.5) in a distance less than 140

km, affecting Tehran, the capital of Iran. We determined several spatial and spatiotemporal slip distributions for this earthquake using different hypocentral parameters (Table 2). Figure 3 illustrates the final slip models in which slip distributions are a little sensitive to the depth of the hypocenter except for the EMSC hypocenter. Among these models, the ISC hypocenter (Table 2) provided the best fit to the observed data with the maximum total variance reduction of 35.30 % for the spatial and 54.50 % for the spatiotemporal distribution. Thus, it was chosen as the preferred spatial slip model for the Kahak earthquake. In Figure 3, the ISC hypocenter is shown with other agencies' hypocenters to demonstrate the relative stability of the main slip zone of all models in relation to the ISC hypocenter location.

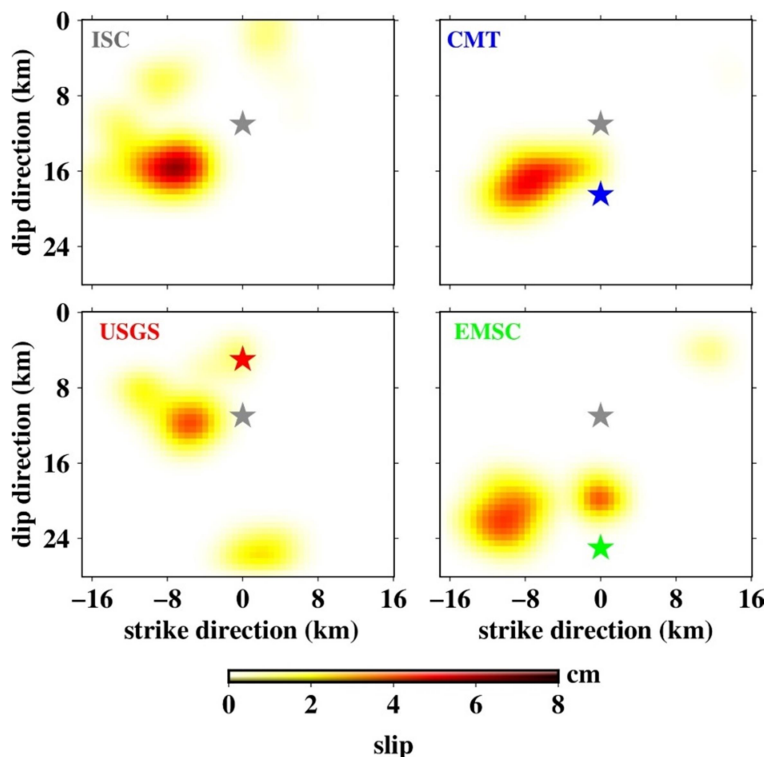


**Figure 3.** A set of spatial solutions for the Kahak earthquake using hypocentral parameters reported by different seismological agencies, which are ISC, GCMT, USGS, and EMSC (see Table 1). The ISC hypocenter is depicted by a gray star in all four sub-figures. We acquired the first model (top, left) using the ISC hypocenter. The model in the top right panel results from the CMT hypocenter, and the blue star displays its hypocenter. Similarly, the models in bottom left (red star) and right (green star) are the results of the USGS and EMSC hypocenters, respectively. As it can be seen in these sub-figures, the main slip zone is approximately placed in the west or southwest of the ISC hypocenter. Our preferred solution is the model resulting from the ISC hypocenter (top, left) with the largest amount of fitting to the data (35.30 % for the spatial and 54.50 % for the spatiotemporal distribution). The peak slip value in all models is scaled to 8.0 cm (the peak slip value of the preferred slip model is about 8.0 cm).

For this event, we used the velocity model introduced by Ashtari et al. (2005), and in so doing, the rupture velocity of 2.6 km/s ( $0.75 V_s$ ) caused the best fit to the data. The optimum rise time was also chosen to be 1.4 s. As it is seen from the preferred model (Figure 3, ISC), the spatial distribution demonstrates an asperity centered southwest of the hypocenter. Furthermore, the total seismic moment of our final model is  $1.59 \times 10^{24}$  dyne-cm ( $M_w \approx 5.8$ ), which concurs with the moment determined from the theory ( $M_0 = \mu A \bar{D}$ ).

Next, we investigated the spatiotemporal slip distribution by applying multiple time window inversion to acquire better data fit. Figure 4 shows a snapshot view of the rupture history with 0.5 s between 6-time steps. As it can be seen in this figure, the western asperity is still predominant with a maximum slip of about 6.0 cm and has

developed during the first 0.5 s of the rupture. Then, the development of the main patch continues until the third step, and thereafter other slip zones start to appear. The seventh sub-figure of Figure 4 is the final spatiotemporal slip distribution of the Kahak event. To clarify the improvement in the multiple time window method, a comparison between the data fit of the spatial and spatiotemporal slip distributions is displayed in Figure 5. Since the multiple time window approach includes time evolution, it yielded, by and large, a better fit to the peak amplitude of each record. However, there is a slight decline in the fit to some records (i.e. CHTH\_BHE, CHTH\_BHN, CHTH\_BHZ, DAMV\_BHN, DAMV\_BHZ, NASN\_BHN), resulting from the low-resolution data. Nevertheless, the spatiotemporal synthetics of these stations are smoother than their spatial synthetics.

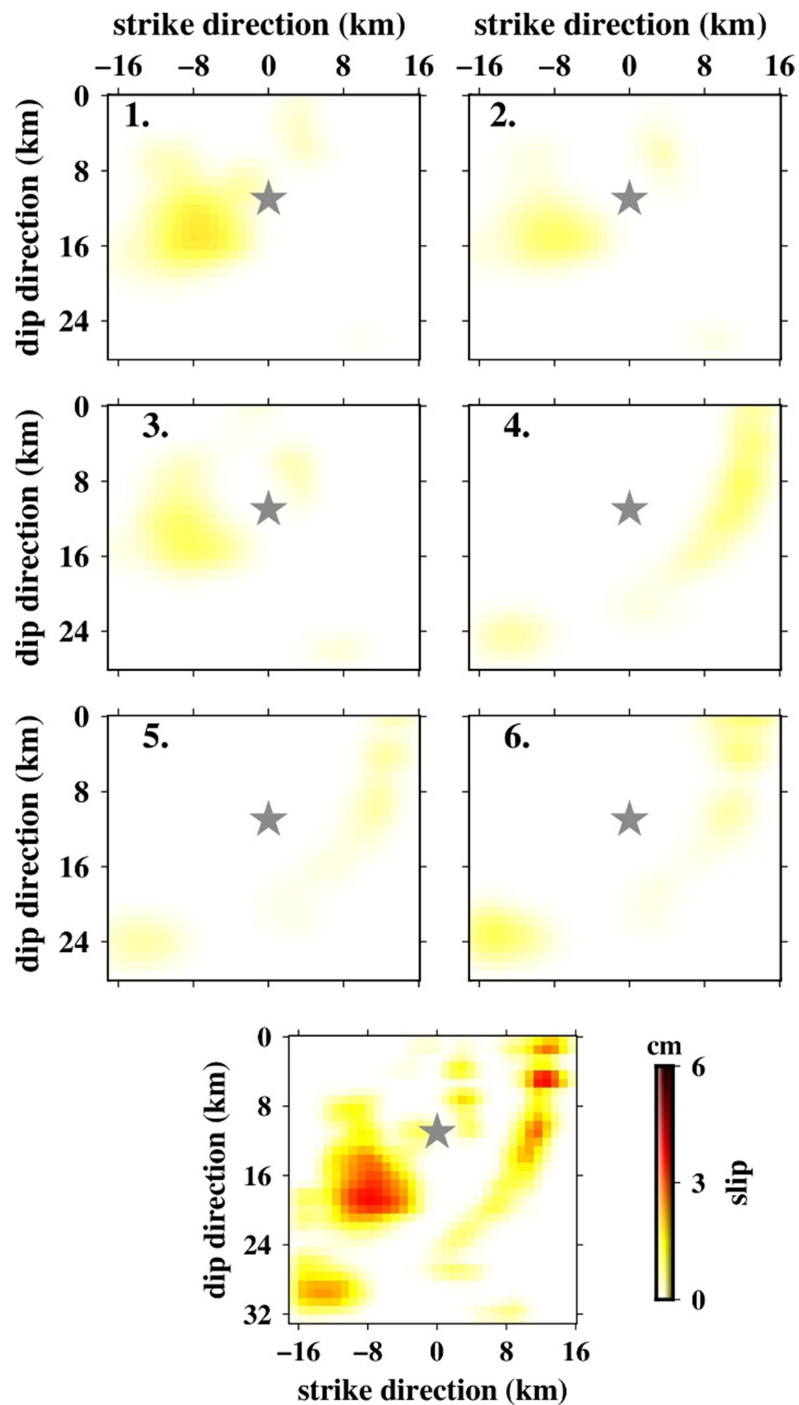


**Figure 4.** Spatiotemporal distribution of the Kahak earthquake. Snapshots of the slip distribution with a 0.5 s time difference between them and the cumulative slip are depicted. The seventh sub-figure shows the final spatiotemporal slip distribution. The gray star displays the ISC hypocenter. The peak slip value in all sub-figures is scaled to 6.0 cm, which is the peak slip value of the spatiotemporal slip distribution of this earthquake.

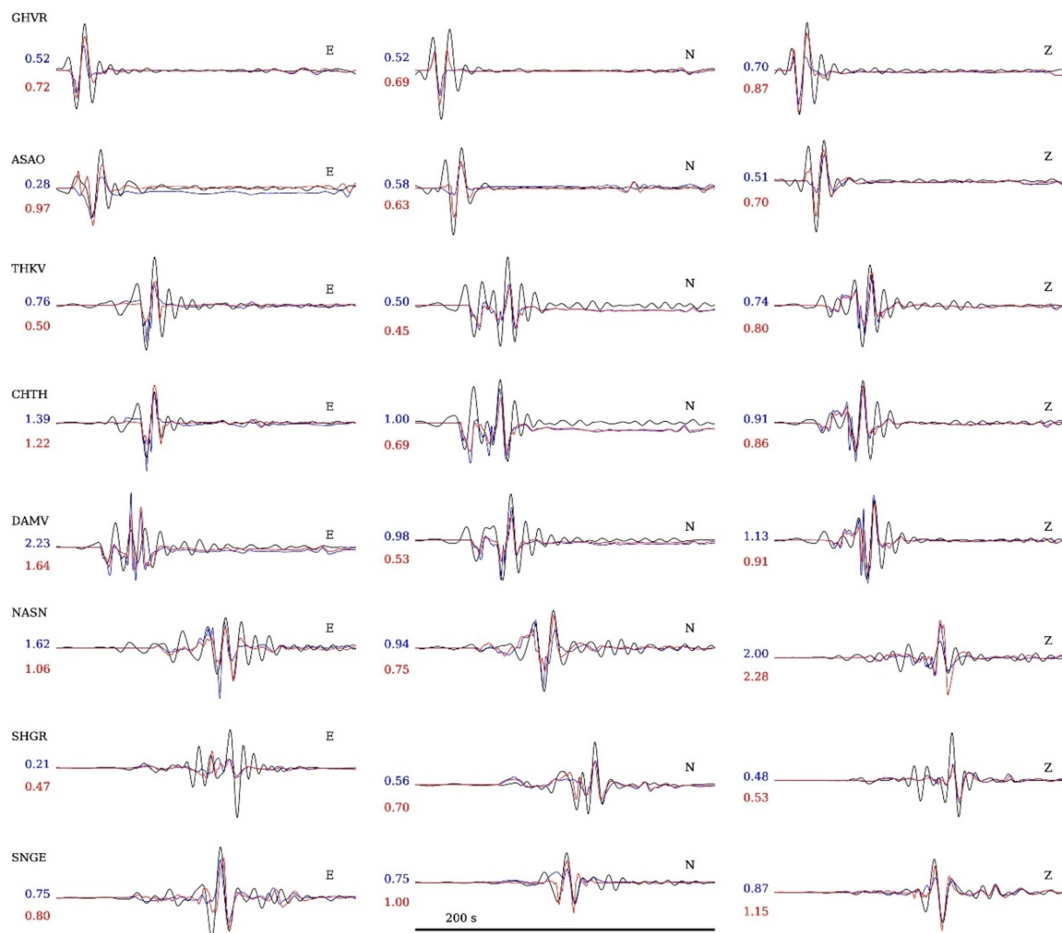


**Figure 5.** Observed data (black) and synthetics (blue and red for spatial and spatiotemporal distribution, respectively) of the final model of the Kahak earthquake. These synthetics with the total variance reduction of 35.30 % (spatial distribution) and 54.50 % (spatiotemporal distribution), generating the final model with the rupture velocity of 2.6 km/s and rise time of 1.4 s, obtained from the ISC hypocenter and the GCMT focal mechanism. Numbers on the left of each signal pair are the synthetic to observed amplitude ratio (blue numbers for the spatial distribution and red numbers for the spatiotemporal distribution). The signals are displayed in order of increasing the distance from the epicenter.

## 5. The results of the 2010 Kazerun Earthquake

The 2010 Kazerun earthquake ( $M_w$  5.9) has been the largest recorded earthquake in the Kazerun region since 2000, and its aftershocks did not exceed the magnitude 4.3. We used the velocity structure based on the study of Hatzfeld et al. (2003) for this earthquake, and 2.8 km/s ( $0.75 V_s$ ) was the optimum rupture velocity. Based on many inversion trials, rupture velocities higher than 2.8 km/s did not explain the rupturing well. The east-west component of the AHRM station was omitted, for the initial 50 s of the waveform did not have an acceptable data fit because of the presence of noise. To acquire the slip distribution of this event (Figure 6), we used different hypocentral parameters (Table 2).

Consequently, the best fit to the observed data (Figure 7) with the maximum total variance reduction of 54.44 % was obtained using the ISC hypocenter, which produced the final slip model for this event. Moreover, the optimum rise time of 2.1 s yielded the best fit to the data. Additionally, the rupture area relationship for reverse slip fault introduced by Wells and Coppersmith (1994) for this earthquake is about  $60 \text{ km}^2$  that is approximately equal to the area of the maximum slip resulting from the ISC hypocenter. Furthermore, the result of the spatiotemporal slip distribution with the total variance reduction of 57 % is not presented here, because a remarkable improvement in the data fit was not acquired (further details are discussed in “the sensitivity of the results”).

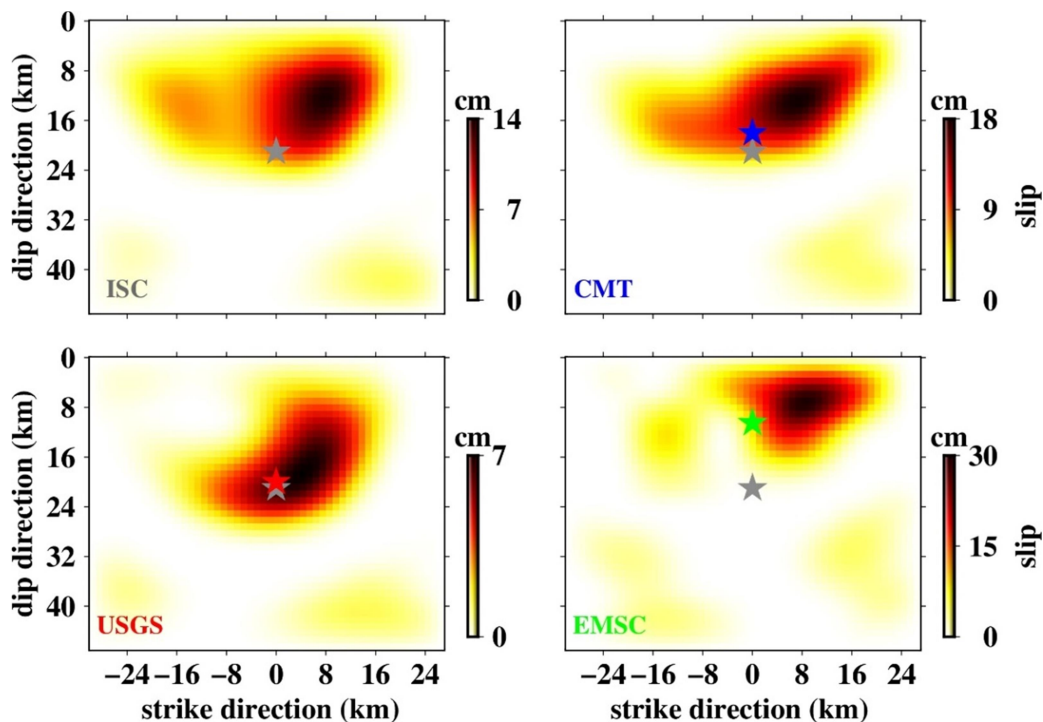


**Figure 6.** A set of solutions for the spatial slip distribution of the Kazerun earthquake using different seismological agencies (ISC, GCMT, USGS, and EMSC (see Table 1)). The ISC hypocenter is shown by a gray star in all solutions. The first model with only the gray star results from the ISC hypocenter. The next three sub-figures illustrate the slip patterns using the CMT hypocenter (top, right) with the blue star, the USGS hypocenter (bottom, left) with the red star, and the EMSC hypocenter (bottom, right) with the green star. Our preferred model for this event is the model resulting from the ISC hypocenter (top, left) with the maximum total variance reduction of 54.44 %.

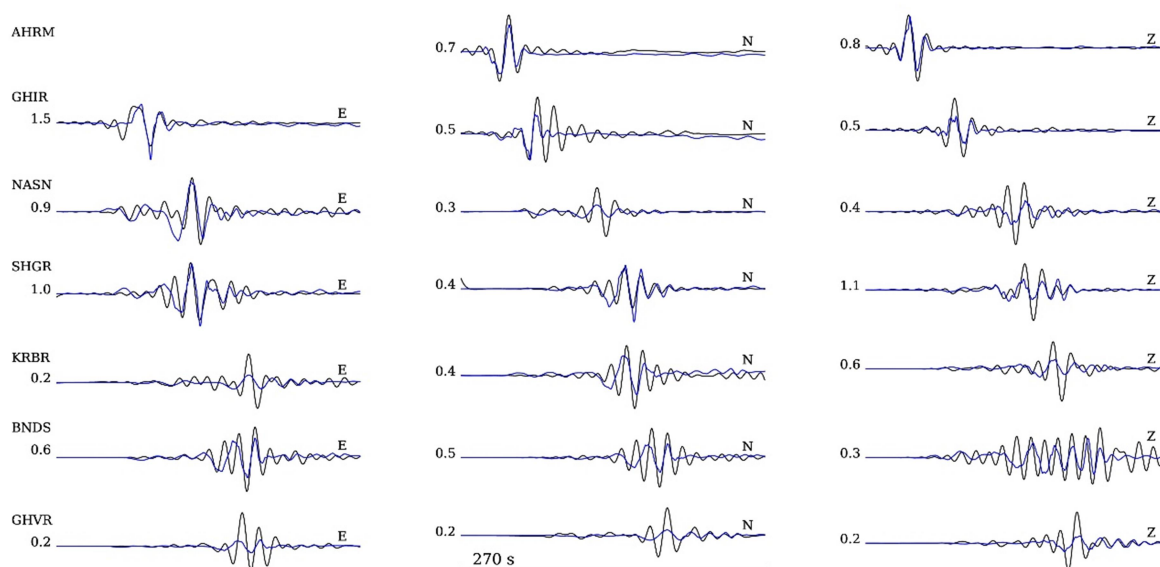


**Figure 7.** Observed (black) and synthetic (blue) data for the spatial slip distribution of the Kazerun earthquake using the ISC hypocenter and GCMT focal mechanism. These signals construct our preferred model with the total variance reduction of 54.44 %, the rupture velocity of 2.8 km/s, and the rise time of 2.1 s. The E component of the AHRM station was omitted, for the presence of noise resulted in an unfavorable synthetic waveform. Numbers on the left of each signal pair show the synthetic to observed amplitude ratio, and signals are arranged in order of increasing the distance from the epicenter.

### 6. The sensitivity of the results

The resulting models from the ISC hypocenters (Figures 3-ISC, 6-ISC) are the ultimate solutions we chose for both earthquakes. In this section, we investigate the influence of some parameters on the rupture history of the final models. These parameters are rupture velocity, rise time, and data sets.

For both earthquakes, we tested different amounts of the rupture velocity ranging from 0.7 to 0.9  $V_s$  (Table 4). According to this test, an increase in the rupture

velocity was followed by the seismic moment growth. Furthermore, the amount of fitting to the data, by and large, was negatively correlated with the rupture velocity, and the peak slip behaved differently for both earthquakes. Moreover, as demonstrated for the Kahak earthquake in Figure 8, a rise in the rupture velocity reduced the area of the maximum slip (dark area). For the Kazerun earthquake, an increase in the rupture velocity caused the slip pattern to be split into two patches (Figure 9).

**Table 4.** The effect of the rupture velocity on the slip models.

Kahak Earthquake				Kazerun Earthquake		
$V_r$ (km/s)	Seismic Moment (dyn-cm)	Total Variance Reduction (%)	Peak Slip (cm)	Seismic Moment (dyn-cm)	Total Variance Reduction (%)	Peak Slip (cm)
0.7 $V_s$	1.54e+24	35.20	8.60	2.79e+25	54.30	13.80
0.75 $V_s$	1.59e+24	35.30	8.57	2.80e+25	54.44	14.26
0.8 $V_s$	1.62e+24	34.81	7.90	2.81e+25	54.39	14.71
0.85 $V_s$	1.63e+24	34.05	7.48	2.82e+25	54.22	14.83
0.9 $V_s$	1.64e+24	33.03	7.26	2.83e+25	53.97	14.65

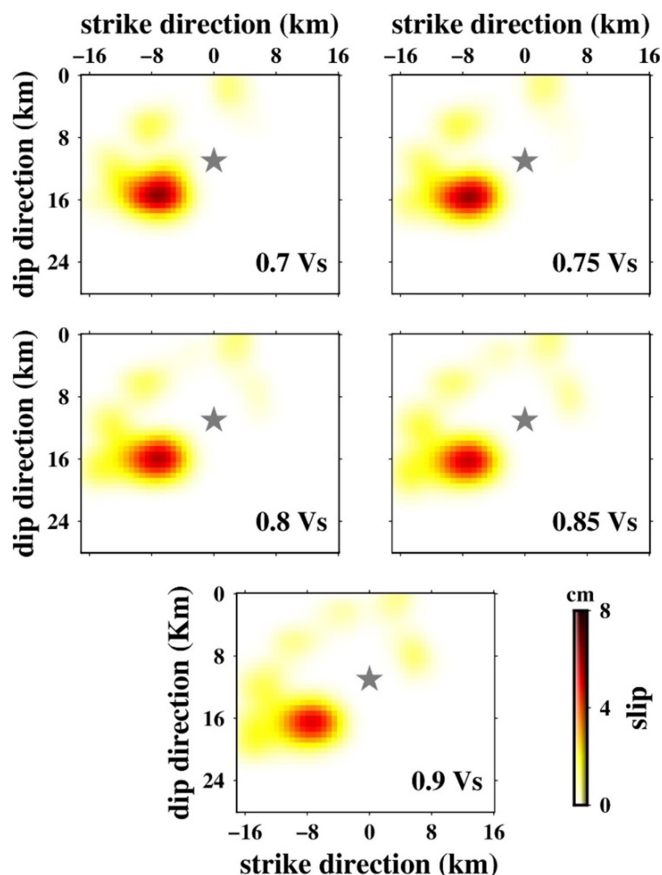


**Figure 8.** The effect of different amounts of the rupture velocity varying from 0.75 to 0.9  $V_s$  on the slip model of the Kahak earthquake. The rise in the rupture velocity increases the seismic moment and decreases the area of the majority of the slip. The gray stars show the ISC hypocenter.

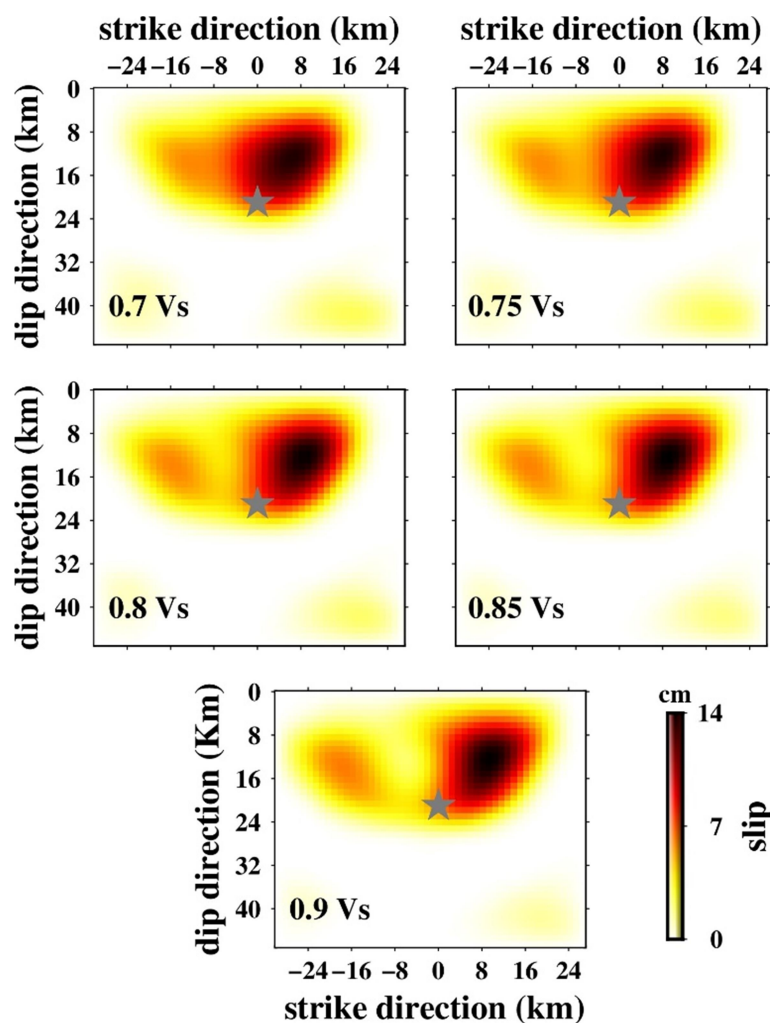


**Figure 9.** The influence of several values of the rupture velocity in the range 0.75-0.9  $V_s$  on the Kazerun slip model. This increase divides the slip pattern into two patches. The ISC hypocenter is illustrated by the gray stars.

Moreover, the rise time was permitted to change from 1.0 to 3.0 s for both earthquakes, which lowered the seismic moment. In addition, the peak slip trended upwards in the first event and downwards in the second one, and the changes in their total variance reduction were small (Table 5). For the Kahak earthquake, as

depicted in Figure 10a, the area of the maximum slip (dark area) increased with the rise time growth, while the whole area of the pattern decreased. For the Kazerun earthquake, increasing the rise time not only caused the distribution to be smaller but also switched the pattern from divided to unified (Figure 10b).

**Table 5.** The effect of the rise time on the slip models.

Kahak Earthquake				Kazerun Earthquake		
Rise Times (s)	Seismic Moment (dyn-cm)	Total Variance Reduction (%)	Peak Slip (cm)	Seismic Moment (dyn-cm)	Total Variance Reduction (%)	Peak Slip (cm)
1	1.60e+24	34.82	8.21	2.85e+25	54.19	15.19
2	1.55e+24	35.58	9.33	2.81e+25	54.46	14.37
3	1.51e+24	34.71	11.07	2.74e+25	54.04	13.40

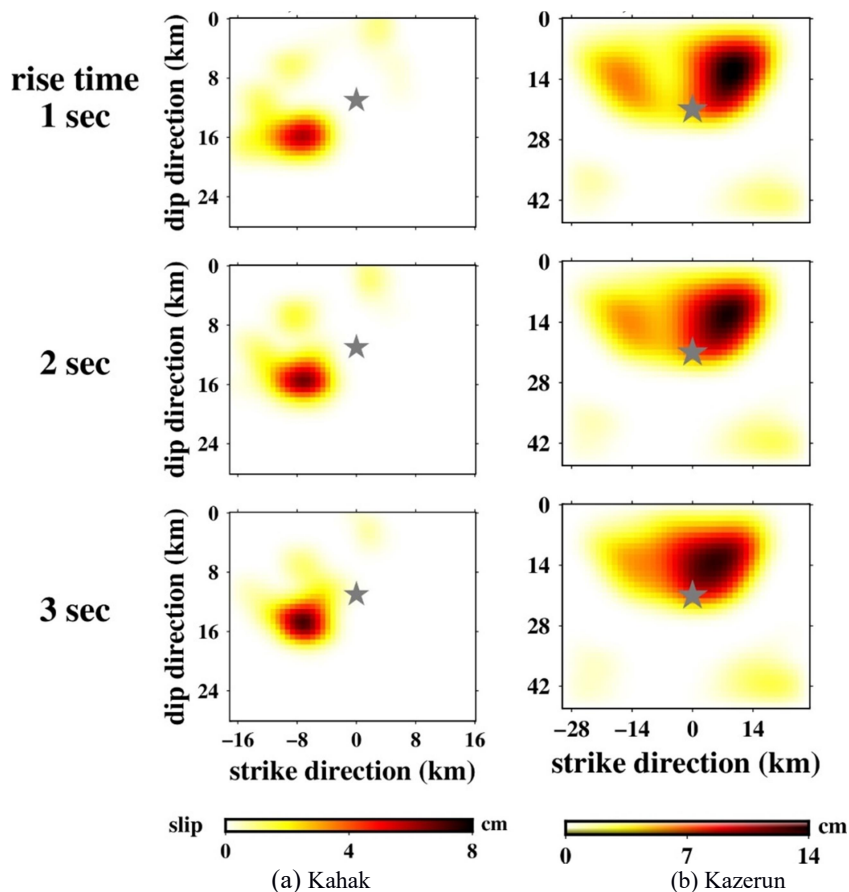


**Figure 10.** The effect of the rise time ranging from 1.0 to 3.0 s on the a) Kahak and b) Kazerun slip models. As the rise time increases, the rupture area decreases. The gray stars display the ISC hypocenter.

Furthermore, we divided stations into different groups and then acquired the data inversion to investigate the sensitivity of the final slip models to the data set. This test can help us analyze the impact of the distribution geometry of stations on the solution. For this mean, two scenarios were defined as follows. First, we conducted the inversion once for a single station and once again for all, but the latter was done by excluding that single one. This procedure was repeated for the whole station. Second, we separated them into two groups of near and far stations based on their epicentral distances (Table 1).

Running the inversion for the spatial distribution of the Kahak earthquake by considering the GHVR station only and once more the ASAO station (the first scenario), we found that the data fit is identical, yet the resulting slip distributions are different. In other words, the slip model resulting from the GHVR station only is more similar to the preferred model and possesses the largest total variance reduction among all experiments of the scenario. The main

conclusion to be drawn from this discussion is that the GHVR and ASAO stations have a strong impact on rupturing for two reasons: They are located not only near the epicenter but also along the fault plane. In addition, the point of this experiment is to investigate the impact of each station on the slip model; therefore, we presented the total variance reduction, the seismic moment, and the total slip percentage changes of the first part of the first scenario in Figure 11. As this figure shows, the worst case is related to implementing the inversion by considering only the SNGE station (the farthest) with about 70 percent reduction in the seismic moment and the total slip. Furthermore, this figure is evidence of less influence of the far stations on the final model, being corroborated by the second scenario in which the GHVR and ASAO (the near stations) formed chiefly the slip pattern. The far stations in the second scenario are THKV, CHTH, DAMV, NASN, SHGR, and SNGE. Applying the first scenario to the Kazerun earthquake indicated that the AHRM station

has the biggest role in forming the final slip distribution. A satisfactory explanation for this dominance is that not only is AHRM the nearest station with the epicentral distance of 95 km, but also its signals' amplitudes are approximately ten times the far ones (NASN, SHGR, KRBR, BNDS, GHVR). For the same reasons, other stations which are the far ones are not a major factor in forming the pattern. Additionally, the GHIR station affects the model not as much as the AHRM station but more than the far ones. The whole experiment explains why this earthquake's spatiotemporal slip distribution could not make improvements in the data fit. The reason is that the AHRM station controlling the slip pattern has a great total variance reduction in the spatial slip model, namely 70 % on average (Figure 7). Thus, there is not much to be changed in the data fit by the multi-time-window method. That is why the time evolution of rupture for the Kazerun earthquake has not been provided here.

## 7. Discussion and Conclusion

The main purpose of this study was to investigate the slip history of the 2007 Kahak ( $M_w$  5.5) and 2010 Kazerun ( $M_w$  5.9) earthquakes using the linear finite-fault slip inversion method. Our analysis was considered at nearly low frequencies and aimed to bring about the main features of the slip distribution of these events. We presented a set of solutions for both

earthquakes; among them, the ISC hypocenter and the GCMT focal mechanism gave the best spatial and spatiotemporal distribution with the maximum total variance reduction of 35.30 % and 54.50 % for the first event (Figures 3, 4, 5, and 12a) and 54.44 % for the spatial distribution of the second event (Figures 6, 7, and 12b). Furthermore, the main nodal planes, recognized in the cross-sectional view, were those planes which provided the maximum total variance reduction in the slip inversion. In addition, the peak slip values of the first and the second events are 8.6 and 14.3 cm, respectively. However, the Wells and Coppersmith (1994) formula between maximum slip and moment magnitude for an earthquake such as the Kazerun event brought about 74 cm, which gives a picture of an expected slip value for this earthquake. The discrepancy between the expected and calculated slip value can be explained by Zagros aseismic behavior, caused by domes and plugs of Hormoz Salt Deformation in the Southern Zagros (e.g. Talbot, 1988), and some extrusions of the salt near the Kazerun fault (e.g. Berberian, 1995; Yamini-Fard et al., 2006). Additionally, a sedimentary cover which was decoupled from the metamorphic basement by the Hormoz Salt leads to aseismic slip (Jackson and McKenzie, 1988; Baker et al., 1993; Berberian, 1995) in this region. Therefore, the salt may control slip in this area and cause a drop in its value.

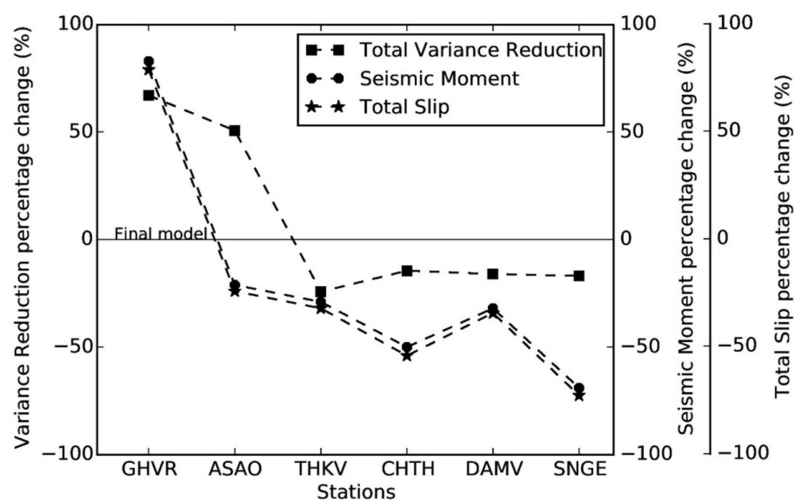


**Figure 11.** Total variance reduction (squares), seismic moment (circles), and total slip (stars) percentage changes of some stations for the first part of the first scenario of the Kahak earthquake. The horizontal line shows the percentage change (0 %) in the final model (Figure 3). Stations are displayed in order of increasing the distance from the epicenter. As the epicentral distance of the stations increases, the values of these three parameters decrease, generally.

Many inversion trials underscore the fact that the rupture velocity plays an indispensable role in the slip inversion. The rupture velocity of 2.6 and 2.8 km/s generated the smoothest synthetic data with the maximum total variance reduction for the Kahak and Kazerun earthquakes, respectively. Also, we re-inverted the observed data for different rupture velocities to investigate their effects on the final models. As the rupture velocity went up, the slip was distributed further out of the hypocenter for the Kazerun earthquake, which is in agreement with the sensitivity test results done by Hartzell et al. (2007) for the 2004 Parkfield, California earthquake. In addition, increasing the rupture velocity increased the seismic moment and decreased the total variance

reduction.

Moreover, other parameters affecting the slip models are at work. One of them is the rise time to which the slip distribution was sensitive. We found 1.4 s and 2.1 s to be the optimum rise times for the Kahak and Kazerun earthquakes, respectively. Different values of this parameter demonstrated that the rise time growth reduces the rupture area and the seismic moment. According to the sensitivity test, slip distribution was also heavily influenced by the number of stations and different sets of data. A similar finding had been acquired by Hartzell et al. (2007) for the 2004 Parkfield, California earthquake. Finally, we draw a comparison between the slip pattern in the fault plane and its projection on the earth's surface (Figure 12).

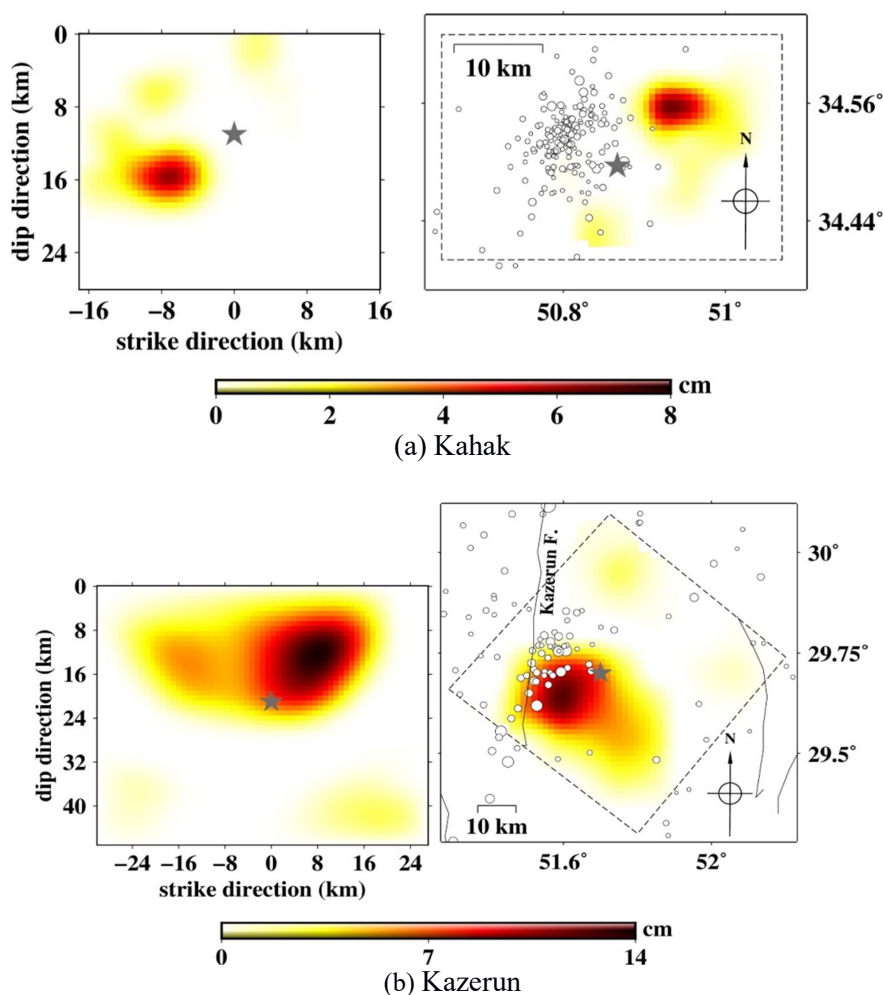


**Figure 12.** Final slip models for the a) Kahak and b) Kazerun earthquakes on the fault plane (left) and the earth's surface (right). The dashed squares (left) illustrate the fault planes on the earth. Gray stars depict the ISC hypocenters for both events. The white circles are the aftershocks during the three months following the main shock, which are taken from the earthquake catalog compiled by the Iranian Seismological Center (IRSC). Generally, the aftershocks distribute outside of the majority of the slip for both earthquakes. Furthermore, the peak slip value of the first and second events are 8.6 and 14.3 cm, respectively.

The goal is to analyze the aftershock location regarding the slip pattern. Since the aftershocks are a phase of relaxing stress concentrations, resulting from the mainshock (Scholz, 1990; Lay and Wallace, 1995), they are expected to spread outside of the slip patch. For the Kahak earthquake, the distribution occurs near the western end of the slip model. There is also a predominance of aftershocks, which surrounds the majority of the slip in the Kazerun model. Therefore, the aftershocks distribute primarily outside of the majority of the slip. This result is supported by studies such as Doser and Kanamori (1986), Hartzell and Heaton (1986), Mendoza and Hartzell (1988), Reasenber and Ellsworth (1982), and Bazargan et al. (2018).

#### Acknowledgment

We would like to appreciate Dr. Mohammad Bigdeli from Iran University of Science and Technology for his help in signal processing. The data are taken from the Earthquake Engineering and Seismology of Iran (IEES) and Iranian Seismological Center (IRSC) for which we are thankful.

#### References

- Abercrombie, R. E., Bannister, S., Panchar, A., Webb, T. H. and Mori, J. J., 2001, Determination of fault planes in a complex aftershock sequence using two-dimensional slip inversion. *Geophys. J. Int.*, 146(1), 134-142.
- Ashtari, M., Hatzfeld, D. and Kamalian, N., 2005, Microseismicity in the region of Tehran. *Tectonophysics*, 395(3), 193-208.
- Baker, C., Jackson, J. and Priestley, K., 1993, Earthquakes on the Kazerun Line in the Zagros Mountains of Iran: strike-slip faulting within a fold-and-thrust belt. *Geophys. J. Int.*, 115(1), 41-61.
- Bazargan, S., Asaadi, N., Shomali, Z. H. and Rezapour, M., 2018, Slip distribution of the 2010 August 27 Mw 5.8 Kuh-Zar earthquake from finite-fault modeling. *IJAA*, 5(1), 41-9.
- Berberian, M., 1981, Active faulting and tectonics of Iran. *Zagros Hindu Kush Himalaya Geodynamic Evolution*, 33-69.
- Berberian, M., 1995, Master "blind" thrust faults hidden under the Zagros folds: active basement tectonics and surface morphotectonics. *Tectonophysics*, 241(3), 193-224.
- Berberian, M. and Tcanlenco, J., 1976, Earthquakes of the southern Zagros (Iran): Bushehr region. *Geol. Surv. Iran*, 39, 343-370.
- Delouis, B., Giardini, D., Lundgren, P. and Salichon, J., 2002, Joint inversion of InSAR, GPS, teleseismic, and strong-motion data for the spatial and temporal distribution of earthquake slip: Application to the 1999 Izmit mainshock. *Bull. Seismol. Soc. Am.*, 92(1), 278-299.
- Doser, D. I. and Kanamori, H., 1986, Depth of seismicity in the Imperial Valley region (1977-1983) and its relationship to heatflow, crustal structure, and the October 15, 1979 earthquake. *J. Geophys. Res.*, 91(B1), 675-688.
- Hartzell, S. H. and Heaton, T. H., 1983, Inversion of strong ground motion and teleseismic waveform data for the fault rupture history of the 1979 Imperial Valley, California, earthquake. *Bull. Seismol. Soc. Am.*, 73(6A), 1553-1583.
- Hartzell, S. H. and Heaton, T. H., 1986, Rupture history of the 1984 Morgan Hill, California, earthquake from the inversion of strong motion records. *Bull. Seismol. Soc. Am.*, 76(3), 649-674.
- Hartzell, S., Liu, P., Mendoza, C., Ji, C. and Larson, K. M., 2007, Stability and uncertainty of finite-fault slip inversions: Application to the 2004 Parkfield, California, earthquake. *Bull. Seismol. Soc. Am.*, 97, 1911-1934.
- Hatzfeld, D., Tatar, M., Priestly, K. and Ghafory-Ashtiany, M., 2003, Seismological constraints on the crustal structure beneath the Zagros Mountain belt (Iran). *Geophys. J. Int.*, 155, 403-410.
- Jackson, J. and McKenzie, D., 1988, The relationship between plate motions and seismic moment tensors, and the rates of active deformation in the Mediterranean and Middle East. *Geophys. J. Int.*, 93(1), 45-73.
- Lay, T. and Wallace, T.C., 1995, *Modern global seismology*. Academic Press, San Diego.
- Mendoza, C. and Hartzell, S. H., 1988, Aftershock patterns and main shock faulting. *Bull. Seismol. Soc. Am.*, 78, 1438-1449.

- Mirzaei, N., Mengtan, G. and Yuntai, C., 1998, Seismic source regionalization for seismic zoning of Iran: major seismotectonic provinces. *J. Earth. Predict. Res.*, 7, 465-495.
- Reasenberg, P. and Ellsworth, W. L., 1982, Aftershocks of the Coyote Lake, California, earthquake of August 6, 1979: A detailed study. *J. Geophys. Res.*, 87(B13), 10637-10655.
- Saikia, C. K., 1994, Modified frequency-wave-number algorithm for regional seismograms using Filon's quadrature-modeling of L(g) waves in eastern North America. *Geophys. J. Int.*, 118, 142-158.
- Scholz, C. H., 1990, The mechanics of earthquakes and faulting. Cambridge University Press, Cambridge, 227.
- Talbot, C. J., 1998, Extrusion of Hormuz salt in Iran. *Geol. Soc. Spec. Publ.*, 143, 315-334.
- Wells, D. L. and Coppersmith, K. J., 1994, New empirical relationships among magnitude, rupture length, rupture width, rupture area, and surface displacement. *Bull. Seismol. Soc. Am.*, 84(4), 974-1002.
- Yamini-Fard, F., Hatzfeld, H., Tatar, M. and Mokhtari, M., 2006, Microearthquake seismicity at the intersection between the Kazerun fault and the Main Recent Fault (Zagros, Iran). *Geophys. J. Int.*, 166, 186-196.